Journal of Catalysis **204,** 466–478 (2001)
doi:10.1006/jcat.2001.3417, available online at http://www.idealibrary.com on IDEAL®

α-TiP-Supported Vanadium Oxide Catalysts: Influence of Calcination Pretreatments on Structure and Performance for *o*-Xylene Oxidation

S. del Val,* M. López Granados,* J. L. G. Fierro,*,[1] J. Santamaría-González,† A. Jiménez López,† and T. Blasco‡

*Instituto de Catálisis y Petroleoquímica, CSIC, 28049 Madrid, Spain; †Departamento de Química Inorgánica, Cristalografía y Mineralogía, Facultad de Ciencias, Universidad de Málaga, 29071 Málaga, Spain; and ‡Instituto de Tecnología Química (UPV-CSIC), Universidad Politécnica de Valencia, Avda. de los Naranjos, s/n, 46022 Valencia, Spain

Received June 15, 2001; revised September 11, 2001; accepted September 17, 2001

The changes induced by increasing the calcination temperature in vanadium oxide supported on α-$Ti(HPO_4)_2H_2O$ (α-TiP) are presented. The characterization on samples calcined at low temperature by TGA, DTA, XRD, XPS, and Raman spectroscopy showed that a mixture of poorly dispersed $VOPO_4$ is present at the surface of α-TiP after calcination. At higher calcination temperatures vanadium does not spread over the surface. On the contrary, a cubic $TiV_xP_{2-x}O_7$ solid solution is formed that induces the migration of V cations into the bulk Ti phosphate and the consequent phosphorous segregation to the surface. The conversion of *o*-xylene to phthalic anhydride is worse on the samples calcined at higher temperatures, and was ascribed to the drastic decrease in the specific surface. The drop in phthalic anhydride selectivity is related to the increase in P concentration at the surface due to the migration of P cations induced by the formation of the solid solution.

Key Words: **vanadium oxide; titanium phosphate; *o*-xylene; selective oxidation; phthalic anhydride; TGA; DTA; XRD; XPS; Raman spectroscopy.**

INTRODUCTION

From the point of view of catalytic properties, the chemical–physical characterization of the V–Ti–P–O system is of interest for two reasons. The first reason is that catalysts based on such systems are currently being studied and tested in several hydrocarbon oxidation reactions to yield products with higher added value. Examples include the oxidation of toluene to benzoic acid (1–3), the oxidation of *o*-xylene to phthalic anhydride (2, 4), the oxidation of ethane to ethene and to acetic acid (5–7), and the oxidation of butane to maleic anhydride (8, 9). The second reason for investigating the V–Ti–P–O system is to shed some light on the controversy concerning the role of P in the catalytic properties of vanadium oxide supported on TiO_2 anatase. This system is of industrial interest due to the replacement of the older naphthalene oxidation process (10, 11) by a new technology based on V_2O_5/TiO_2 catalysts to obtain phthalic anhydride (PA) by oxidation of *o*-xylene. P is an impurity in commercial TiO_2(a) and is very difficult to remove by washing (2). Although P has also been reported to be an impurity in industrial catalysts (4, 12), several patents claim that the incorporation of phosphorus, which is usually concentrated at the surface (13), is beneficial for the catalytic properties (14). Nevertheless, the question as to whether P should be considered, from the catalytic point of view, as an impurity, a promoter, or a poison is still an area of controversy (2, 15–17).

In the V–Ti–O system, the same state of V_2O_5/TiO_2 catalysts is attained when the precursor is calcined or treated under reaction conditions, irrespective of the V addition method (18), as long as other variables such as the composition or calcination temperature are the same and the system has reached chemical equilibrium. The final result is that V_2O_5 wets the TiO_2 surface through a strong interaction between the TiO_2 surface and the VO_x moieties (18–23) if the catalyst is prepared by either chemical vapor deposition, grafting with vanadyl chloride or vanadium alkoxides (24, 25), or incipient wetness or wet impregnation of any vanadium-containing salt (26). Indeed, solid-state reactions between V_2O_5 and anatase (heating at common calcination temperatures a physical mixture of the two oxides) leads to the migration of the V_2O_5 phase over the TiO_2 (support).

However, for the V–Ti–P–O system many V–P–O and Ti–P–O phases have been described in the literature (27–31). More than a decade ago we observed that the impregnation of TiO_2 with P results in the formation of Ti hydrogen phosphate (32). We subsequently used the hydrated titanium hydrogen phosphate, α-$Ti(HPO_4)_2H_2O$ (α-TiP), as a support for vanadium oxide. This solid has already received much attention and has been characterized in detail (33–37), thus providing an insight into the role of P in the catalytic properties of the V–Ti–O system.

[1] To whom correspondence should be addressed. Fax: +34 91 585 4760. E-mail: jlgfierro@icp.csic.es.

0021-9517/01 $35.00

In our previous communication it was shown that vanadium oxide does not spread over the Ti phosphate surface when the precursor resulting from the wet impregnation of α-TiP with a vanadyl oxalate solution is calcined at 723 K (15). Small crystals of α_I-$VOPO_4$ were detected by Raman spectroscopy at low V loading levels, whereas V_2O_5 crystallites were observed at higher V loadings. However, all evidence indicated that such phases were not supported on Ti phosphate, and the system was better described as a physical mixture of Ti phosphate crystals and crystallites of vanadium oxide (or phosphate, depending on the V loading). The uncovered Ti phosphate surface was found to be responsible for the modest catalytic performance.

In the work described here, we increased the calcination temperature (above 723 K) of the materials prepared by wet impregnation of α-TiP with a vanadyl oxalate solution. The aim of this treatment was to determine whether thermal activation could cause spreading of the vanadium phases over the Ti phosphate surface. The V_2O_5/α-TiP catalysts calcined at several temperatures were characterized by a variety of spectroscopic techniques and tested in the oxidation reaction of *o*-xylene. The results strongly suggest that upon increasing the calcination temperature, vanadium is incorporated within the structure of titanium phosphate. The catalytic activity also undergoes drastic changes that are closely related with the structural changes brought about by changing the calcination temperature.

EXPERIMENTAL

Catalyst Preparation

The support, α-$Ti(HPO_4)_2H_2O$ (α-TiP), was prepared by a sol–gel method described elsewhere (15). Catalysts containing a theoretical loading of 10 wt% V_2O_5 were prepared by wet impregnation of α-TiP with an aqueous solution of V_2O_5 (Fluka) in oxalic acid (Panreac) (2.3 g oxalic acid dihydrate/g V_2O_5). This blue solution was prepared by careful addition of V_2O_5 to an aqueous solution of oxalic acid at 323 K under vigorous stirring. The excess water was removed using a rotary evaporator, and the resulting solid was dried (12 h at 333 K) and calcined for 5 h at 723, 823, 923, and 1023 K. The catalysts are referred to as c723, c823, c923, and c1023, respectively, and the catalyst precursor is denoted as 10VTiP. This V oxide loading represents ca. 2.5 theoretical monolayers of V_2O_5 (calculated by geometric considerations on the assumption that the entire support area is available to disperse vanadium oxide), which means that if V_2O_5 could spread over the surface, there would be more than 2.5 monolayers of V_2O_5 covering the support. As a reference, the bare support was calcined at 723, 823, 923, and 1023 K. The samples were denoted as α-TiPc723, α-TiPc823, α-TiPc923, and α-TiPc1023, respectively.

Catalyst Characterization

Chemical analysis of the samples to determine the P, Ti, and V composition was carried out by ICP using a Perkin–Elmer Optima 3300DV apparatus. Nitrogen adsorption experiments were performed at liquid nitrogen temperature (77 K) using a Micromeritics ASAP 2000 apparatus. Prior to the determination of an adsorption isotherm, the sample (approximately 0.25 g) was degassed at 413 K for 24 h. X-ray diffraction (XRD) measurements were performed on a Seifert XRD300 diffractometer using Cu$K\alpha$ radiation by collecting each point for 5 s ($2\theta = 0.04^\circ$). Raman spectra were recorded using a Renishaw 1000 spectrophotometer equipped with a cooled CCD detector (200 K) and a holographic Notch filter that removes the elastic scattering. The samples were excited with the 514-nm Ar line in an *in situ* cell (Linkam, TS-1500), which allows temperature treatments up to 1773 K with different flowing gases. The acquisition of spectra consisted of five accumulations of 60 s for each sample. All the catalysts for the measurements were pretreated *in situ* with an air flow of 100 mL/min (standard temperature and pressure, STP) at 523 K for 30 min prior to recording the spectra.

Thermogravimetric analysis (TGA) was carried out using a Perkin–Elmer TGA-7 apparatus. The samples (ca. 15 mg) were loaded and heated under a flow of dry air at a rate of 40 mL/min and a heating rate of 10 K/min. Thermal differential analysis was performed using a Perkin–Elmer DTA-T apparatus. The samples (ca. 40 mg) were heated under a flow of dry air at a rate of 100 mL/min and a heating rate of 10 K/min.

(X-ray photoelectron spectra XPS) were acquired with a VG Escalab 200R spectrometer equipped with a hemispherical electron analyzer and a Mg$K\alpha$ X-ray source ($h\nu = 1253.6$ eV, 1 eV $= 1.6302 \times 10^{-19}$ J). Powder samples were pressed into small aluminium cylinders and then mounted on a sample rod that was placed in the pretreatment chamber. The samples were then degassed at 298 K for 1 h. The base pressure in the ion-pumped analysis chamber was maintained below 2×10^{-9} mbar during data acquisition. Peak intensities were estimated by calculating the integral of each peak after smoothing and subtraction of the "S-shaped" background, then fitting the experimental curve by a least-squares routine, supplied by the instrument manufacturer, using Gaussian and Lorentzian lines. Atomic ratios were computed from the intensity ratios normalized by atomic sensitivity factors (38). The binding energy (BE) reference was taken at the P 2p peak at 133.3 eV. An estimated error of $\pm$ 0.1 eV can be assumed for all measurements.

^{31}P and ^{51}V nuclear magnetic resonance (NMR) spectra were recorded at room temperature with a Varian VXR S 400WB spectrometer working at 161.9 and 105.1 MHz, respectively, using a 4-mm XC4 Doty probe. Samples were packed into silicon nitride rotors. To acquire the ^{31}P spectra

the samples were spun at magic angle spinning (MAS) rates of ca. 16 kHz, using $\pi/2$ rad pulses of 5 μs and recycle delays of sufficient length to ensure the total recovery of magnetization. The longitudinal relaxation time T_1 of ^{31}P was found to be as long as ca. 550 s for some peaks in the spectrum of the catalyst calcined at 1173 K. ^{51}V solid-state NMR spectra were recorded under static and spinning conditions with pulses of 1 μs, which correspond to a flip angle of $\pi/18$ rad, to avoid distortions of the line shapes and relative intensities of the signals arising from varying degrees of excitation selectivity. A 1-s recycle delay was used to acquire spectra. The ^{51}V MAS NMR spectra were recorded at spinning rates in the 7- to 16-kHz range. In this work we present only the spectra obtained at lower rates. These spectra were selected in order to avoid the phasing problems found in some cases in which faster rates were employed. The ^{51}V chemical shifts were referenced to liquid $VOCl_3$ with $Mg_3(VO_4)_2$, which has a chemical shift of -554 ppm, as a secondary reference. An aqueous solution of $NaVO_3$ was used to calibrate the radiofrequency power.

Catalytic Measurements

Catalytic activity measurements were carried out in a plug-flow glass fixed-bed reactor heated by a cylindrical oven. A sample of approximately 0.250 g (W/F = 179 g · s/L) of catalyst diluted seven times in Carborundum was loaded (particle size: 0.42–0.50 mm). Gas flows were controlled by mass flow controllers. *o*-Xylene (Fluka > 99%) was fed into the system as a liquid by means of a perfusion pump. Alkyl-aromatic and O_2 molar concentrations in the feed were 0.8 and 20.8%, respectively (balance N_2). The inlet lines were heated to 453 K to ensure the evaporation of the alkyl-aromatic compound. A gas chromatograph (GC) (Varian Star 3400 CX) was connected on line with the reactor outlet to analyze permanent gases and volatile fractions of the reaction mixture. An ice-bath trap was placed between the GC and the reactor outlet in order to condense a proportion of the unreacted alkyl-aromatic compounds and the products. The lines connecting the reactor and the trap were heated to 523 K. The temperature of the bottom part of the reactor, which was downstream from the catalyst bed and upstream from the ice trap, was higher than 600 K. The GC was equipped with a thermal conductivity detector (TCD) and a flame ionization detector (FID). Permanent gases (O_2, N_2, H_2O, CO, and CO_2) and gaseous fractions of organic compounds were analyzed by on-line injections. The rest of the products, which were condensed in the ice trap, were dissolved in acetone and analyzed by syringe injection. O_2, H_2O, CO, and CO_2 were separated by two packed columns connected in series (HayeSep D and 5 Å molecular sieves). Organic products were separated by an RTX-5 capillary column.

RESULTS AND DISCUSSION

To investigate the influence of vanadium on the phases formed, the layered α-TiP used as the support and the catalyst precursor calcined at increasing temperatures were characterized by several techniques.

TGA–DTA

Figures 1 and 2 show the TGA and differential thermal analysis (DTA) curves of the support and catalyst precursor. Figure 1 displays the mathematical derivative of the TGA trace for a better discrimination of weight-change processes occurring during heating. The weight losses, recorded up to 450 K for the unloaded support, and the catalyst precursor correspond to the loss of surface-sorbed and crystal water. The second weight loss occurring in the support in the 630–840 K range, which is also observed for the catalyst precursor, is due to the condensation of the PO_3–OH groups present in the interlayer region, a process that causes the transformation of layered α-TiP to layered pyrophosphate L-TiP_2O_7. The main weight loss in the catalyst precursor [10.6% according to Fig. 1(i)] occurs between 466 and 571 K and is due to CO_2 release (decomposition of oxalate) according to

$$4VO(C_2O_4) + 3O_2 \rightarrow 2V_2O_5 + 8CO_2. \qquad [1]$$

Assuming that the first and third weight losses of the catalyst precursor are due to the removal of water and the second one to the evolution of CO_2, the differential thermal analysis (DTA) peaks (Fig. 2) up to ca. 840 K can be easily understood. The peak below ca. 450 K and that appearing in the 630–780 K range, both of which are endothermic, are due to loss of water, while the exothermic peak between 466 and 571 K can be ascribed to the heat release associated with the reaction described by Eq. [1]. The DTA

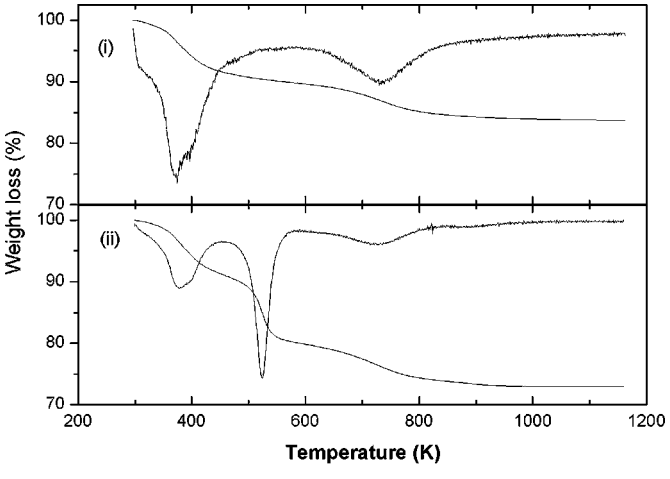

FIG. 1. TG analysis under a flow of air and derivative curves of (i) precursor 10VTiP and (ii) α-$Ti(HPO_4)_2H_2O$ support.

curve of the α-$Ti(HPO_4)_2H_2O$ support shows two broad endothermic peaks at 526 and 570 K with no associated mass loss. These peaks correspond to the α-TiP $\rightarrow$ ξ-TiP and ξ-TiP $\rightarrow$ η-TiP phase transformations, respectively, in the anhydrous-layered phosphate (36).

The high-temperature peaks in the DTA curves of the support and the catalyst precursor are not linked to any weight loss. The DTA profile of α-TiP reveals the transformation of L-TiP_2O_7 to cubic C-TiP_2O_7, which is evidenced by an exothermic peak between 1040 and 1150 K. The most remarkable feature is the very clear decrease in the temperature range at which the L- to C-TiP_2O_7 phase transition occurs in the catalyst precursor (856–997 K), a situation in agreement with our previous results (15). Moreover, the ATD peak of the catalyst precursor shows a different profile than that of the unloaded support, indicating that V promotes, but also alters, the transformation of the layered phase to the cubic phase. Finally, a weak endothermic peak recorded at 1216 K for the α-$Ti(HPO_4)_2H_2O$ support can be ascribed to the melting of the support.

N_2 Adsorption Isotherms

The influence of V is also observed on the surface area and sorption properties of the samples. The specific areas are compared in Table 1. The N_2 adsorption isotherms of the α-TiP support calcined at 723, 823, 923, and 1023 K as well as the catalysts c723 and c823 are of type IV (IUPAC classification) with a hysteresis loop of type H3. This indicates the existence of mesoporosity (39). The hysteresis loop was extremely narrow and appears at very high P/P^0 values. This indicates that capillary condensation takes place between particles (aggregates of particles) and that intraparticle mesoporosity is irrelevant. The catalysts have a lower specific area than the support calcined at the same temperature. Indeed, a marked decrease is observed for c923 and c1023 (see Table 1). For these two catalysts, the N_2 adsorption isotherms change to type II, representing an unrestricted monolayer–multilayer adsorption typical of macroporous or nonporous solids (39). Since the specific area of the α-TiP support calcined at 923 and 1023 K decreases only slightly (see Table 1), the remarkable change in the N_2 adsorption properties of catalysts c923 and c1023 must be related to the presence of V in the catalysts.

TABLE 1

Specific Surface of Catalysts and Support Samples Calcined at Different Temperatures

Sample	S_{BET} (m^2/g)
α-TiPc723	30
c723	17
α-TiPc823	29
c823	10.0
α-TiPc923	26
c923	2.1
α-TiPc1023	24
c1023	1.2

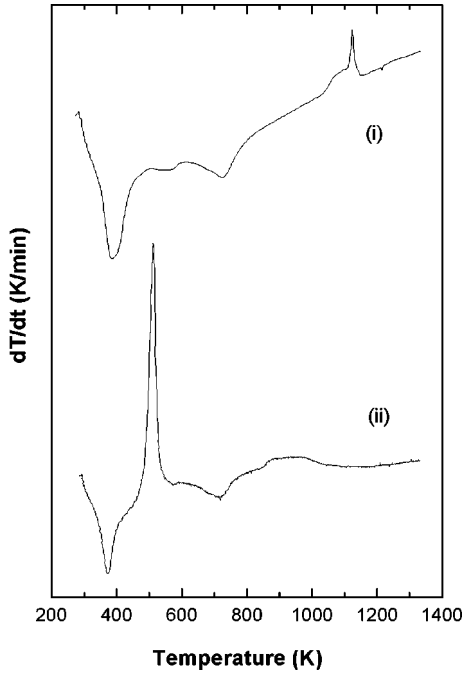

FIG. 2. DTA traces of (ii) precursor 10VTiP and (i) α-$Ti(HPO_4)_2H_2O$ support under a flow of air.

XRD

The X-ray diffraction patterns of α-TiP and catalysts calcined at different temperatures are presented in Figs. 3a and 3b. All reflections are indexed to α-$Ti(HPO_4)_2H_2O$ (40), although the low intensity and broad shape of the patterns indicate poor crystallization of this phase. The diffractogram of the α-TiPc723 sample shown in Fig. 3a contains broad peaks ascribed to the ill-crystallized L-TiP_2O_7 phase. The disorder in the precursor α-TiP must be partially transmitted to the layered pyrophosphate (L-TiP_2O_7), although the dehydration process could introduce further defects in the crystals (see ^{31}P MAS NMR results). Significant changes are not observed upon increasing the calcination temperature to 1023 K. At this temperature reflections that are typical of C-TiP_2O_7 appear [see Fig. 3a(v)].

Peaks of cubic titanium pyrophosphate are observed in the XRD patterns of the catalysts c823, c923, and c1023; i.e., the lower calcination temperature gives rise to a mixture of the support and L- and C-cubic titanium pyrophosphate in c723. These facts agree with the results of DTA, which show that V promotes the transformation of layered to cubic pyrophosphate. It must be pointed out that diffraction lines arising from V phases (V_2O_5 or VPO phases) were not observed by XRD, in agreement with previous findings for samples with higher V loadings (15).

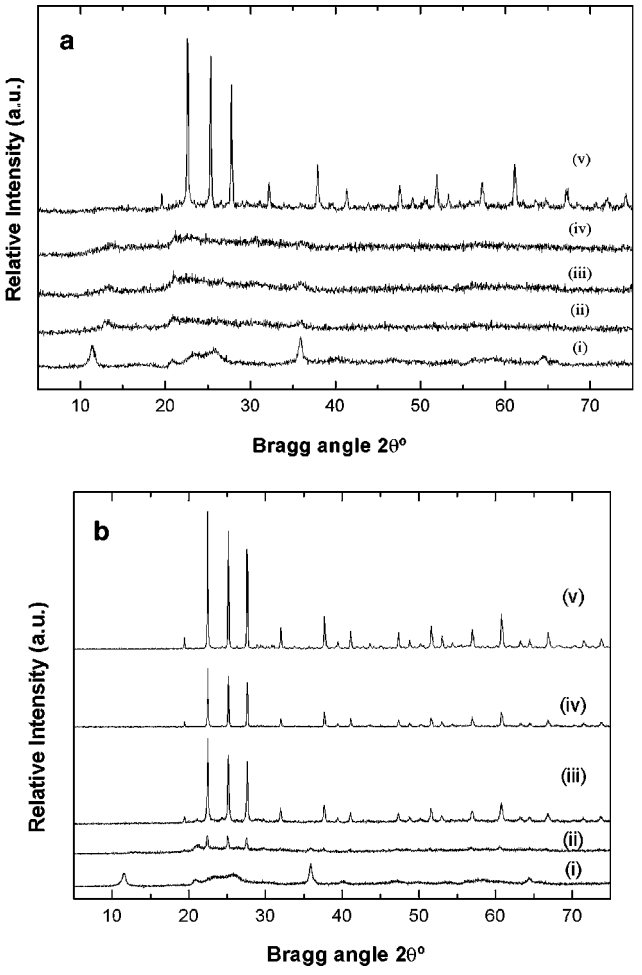

FIG. 3. (a) X-ray diffraction patterns of bare uncalcined support: (i) α-$Ti(HPO_4)_2H_2O$, (ii) α-TiPc723, (iii) α-TiPc823, (iv) α-TiPc923, and (v) α-TiPc1023. (b) X-ray diffraction patterns of (i) precursor 10VTiP, (ii) c723, (iii) c823, (iv) c923, and (v) c1023 K.

A careful examination of the XRD pattern reveals that in vanadium-containing samples, the reflections assigned to C-TiP_2O_7 are shifted to a lower 2θ angle. The C-TiP_2O_7 phase crystallizes in the cubic system within the Pa3 spatial group [cell edge $a = 23.6342(9)$ Å] (41). The cell edge parameter and error bars for the C-TiP_2O_7 phases present in c723, c823, c923, c1023, and c1173 are displayed in Fig. 4. This figure also contains the cell parameter of the α-TiPc1023 support, which is slightly higher than the value reported in (41). In spite of the large error bars due to the relatively short recording time and the ill-crystallization of some samples (catalyst c723), Fig. 4 clearly demonstrates that the lattice parameter of the V-containing catalysts is larger than that of the cubic pyrophosphate phase of the support. This situation is consistent with an expansion of the cubic unit cell, suggesting that V is incorporated into the cubic titanium pyrophosphate phase. The transformation of the layered L-TiP_2O_7 into the cubic form can be accompanied by the formation of a $TiV_xP_{2-x}O_7$-type solid solution, where V(V) occupies tetrahedral P(V) sites in the cubic titanium pyrophosphate lattice. The substitution of P cations (0.34 Å) by the more voluminous V cations (0.59 Å) results in an expansion of the unit cell, a larger distance between diffraction planes, and therefore smaller Bragg angles. The existence of the $ZrV_{2-x}P_xO_7$ solid solution, which is readily prepared from mixtures of precursors of ZrO_2, V_2O_5, and P_2O_5 (42), has been demonstrated. However, to the best of our knowledge, neither the formation of the $TiV_xP_{2-x}O_7$ solid solution nor the synthesis of TiV_2O_7 ($x = 2$) has been reported previously. The preparation method presented in this work opens a new route for the synthesis of such systems. The substitution of Ti^{4+} cations by V^{4+} cations seems very unlikely because XPS did not reveal the presence of significant amounts of V^{4+}(catalysts were of an intense yellow-orange color) and also because such a substitution should require a reducing atmosphere rather than air treatment. The hypothesis of the formation of a solid solution is further supported by other spectroscopic techniques and will be reviewed under Discussion. The remarkable decrease in the phase-change temperature from layered to cubic must be driven by the formation of the seemingly very stable C-$TiV_xP_{2-x}O_7$ solid solution. Figure 4 also shows that the lattice parameter for the $TiV_xP_{2-x}O_7$ solid solution decreases slightly as the calcination temperature increases and then almost levels off when calcination takes place at 1173 K.

Raman Spectroscopy

Besides the cubic pyrophosphate solid solution, XRD data did not reveal the presence of V phases. However, new phases with vanadium can be formed that cannot be detected by XRD because of their crystallization disorder or their very small crystal size. These phases with very small

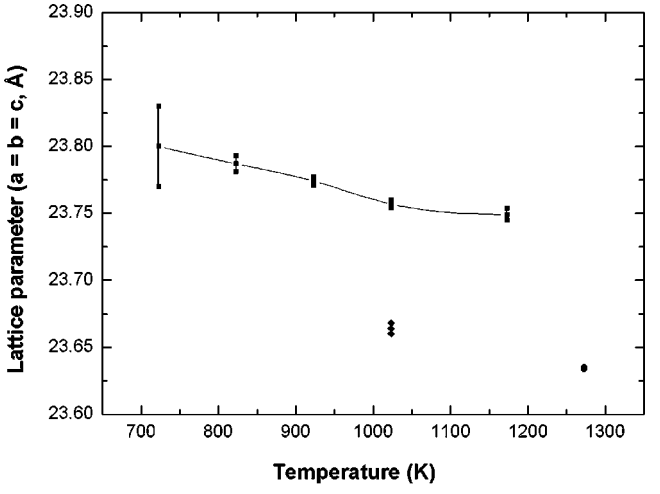

FIG. 4. Dependence of cell edge in solid solution C-$TiV_xP_{2-x}O_7$ with calcination temperature of catalyst. ■, catalysts; ◆, α-TiPc1023; ●, reported data in the literature (41).

crystal size and poor crystallization can be observed by Raman spectroscopy (43). Figure 5a displays the Raman spectra of the α-TiP support calcined at 723, 823, 923, and 1023 K, and Fig. 5b shows the spectra of the different catalysts. Before collecting the Raman spectra, the samples were dehydrated *in situ* by heating in air at 523 K. Table 2 summarizes the Raman features observed. As can be seen from Fig. 5a, the support, regardless of the calcination temperature, displays Raman features in the 100- to 1400-cm^{-1} region. The Raman spectrum of α-TiPc723 is very similar to that of the α phase α-$Ti(HPO_4)_2H_2O$ (36), although the dehydration process results in a lowering of the crystallinity and, therefore, in the broadening of the Raman lines. The Raman spectra of α-TiPc823 and α-TiPc923K are similar to the spectrum of α-TiPc723, indicating that these samples should essentially consist of L-TiP_2O_7, which is consistent with the XRD patterns of those samples (see Fig. 3b). The Raman spectrum of the support calcined at the higher temperature (1023 K), which is presented in Fig. 5a, shows a much more complex and better resolved spectrum than L-TiP_2O_7, especially at lower Raman shifts. Moreover, the most intense lines at 1039 (very strong, vs) and 1069 (shoulder, sh) cm^{-1} are much narrower. All these facts point to a better crytallization of the phase present in the α-TiPc1023 sample. Since cubic C-TiP_2O_7 is the only phase detected by XRD (see Fig. 3b and Table 2), the Raman spectrum shown in Fig. 5a accounts for this phase.

TABLE 2

XPS V/Ti and P/Ti Atomic Ratios of Catalysts Compared to V/Ti and P/Ti Bulk Ratios (Determined by Chemical Analysis)

Catalyst	V/Ti atom XPS	V/Ti atom bulk	P/Ti atom XPS	P/Ti atom bulk
c723	0.42	0.32	3.49	2.10
c823	0.60	0.32	3.36	2.10
c923	0.94	0.32	3.98	2.10
c1023	1.38	0.32	4.22	2.10

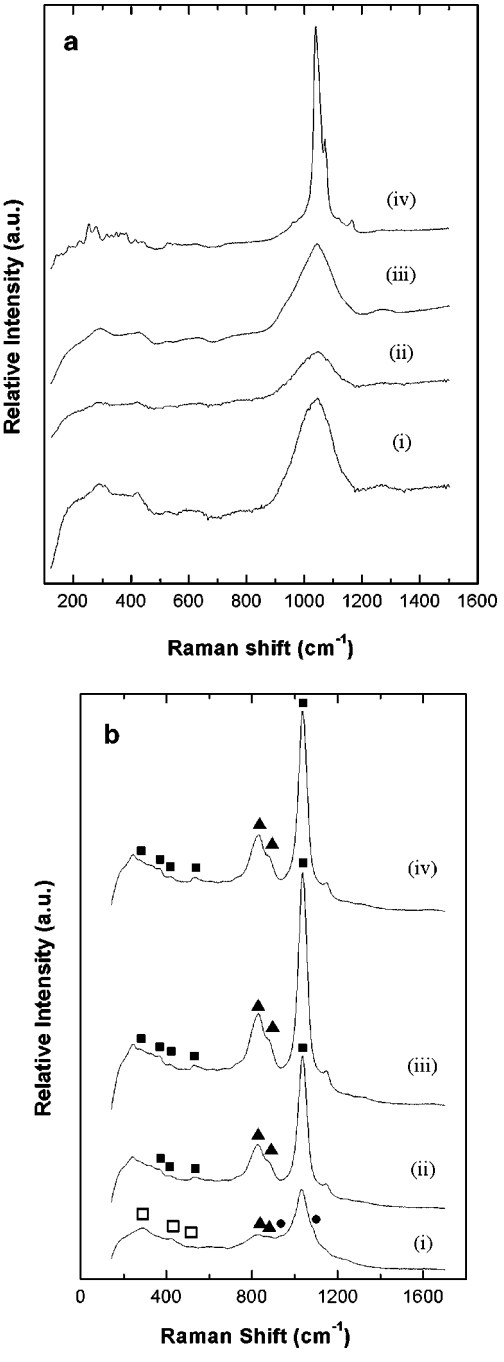

FIG. 5. (a) Raman spectra of support samples: (i) α-TiPc723, (ii) α-TiPc823, (iii) α-TiPc923, and (iv) α-TiPc1023. (b) Raman spectra of catalysts: (i) c723, (ii) c823, (iii) c923, and (iv) c1023. □, L-TiP_2O_7; ▲, C-$TiV_xP_{2-x}O_7$; ●, α_{II}-$VOPO_4$.

In accordance with the XRD patterns, the Raman spectrum of catalyst c723 must be assigned to a mixture of L-TiP_2O_7 and C-$TiV_xP_{2-x}O_7$ phases (see Table 3). Two very weak bands at 940 and 1091 cm^{-1} coincide with the position of the most intense bands of the α_{II}-$VOPO_4$ phase (27, 44), suggesting the formation of this vanadium phosphate in the catalyst. Other intense or medium bands (995 and 979 cm^{-1}) of α_{II}-$VOPO_4$, which are not detected in the spectrum of sample c723, are obscured by the Raman bands of the phosphate phase. Indeed, all of the characteristic features of the phase α_{II}-$VOPO_4$ appear in the spectrum of the nondehydrated sample of c723 (not shown here) (27, 44), which provides further evidence for our assignment. In our previous work (15), α_I-$VOPO_4$ was proposed on the basis of the Raman spectrum of the catalyst c723. However, these new results demonstrate that α_{II} is a more precise assignment.

The Raman spectra of the catalysts calcined at higher temperatures, i.e., c823, c923, and c1023, are quite similar to that of the α-TiPc1023 sample, indicating the presence of a cubic pyrophosphate phase. This situation, in agreement with the XRD data, must correspond to the formation of the $TiV_xP_{2-x}O_7$ solid solution. The catalysts show

TABLE 3

Summary of Raman Bands Positions for Samples of Support and Catalysts [a]

Sample	Raman band positions (cm^{-1})	Assignment
α-TiPc723	287 (m), 421 (m), 523 (vw), 1046 (vs, vb)	□ L-TiP_2O_7
α-TiPc823	287 (m), 421 (m), 523 (vw), 1049 (vs, vb)	□ L-TiP_2O_7
α-TiPc923	290 (m), 429 (m), 526 (vw), 625 (vw), 1043 (vs, vb)	□ L-TiP_2O_7
α-TiPc1023	138 (vw), 157 (vw), 182 (vw), 224 (w), 254 (m), 279 (m), 317 (vw), 347 (vw), 361 (vw), 379 (vw), 415 (vw), 445 (vw), 526 (vw), 958 (w), 1039 (vs), 1069 (sh), 1119 (vw), 1165 (m)	■ C-TiP_2O_7
c723	□ 289 (m), □ 423 (w), □ 520 (vw), ▲ 830 (s), ▲ 870 (sh), ● 940 (m), 1030 (vs), ● 1091 (sh, vw)	□ L-TiP_2O_7, ● α_{II}-$VOPO_4$, ▲ $TiV_xP_{2-x}O_7$
c823	242 (m), 323(vw), ■ 365 (w), ■ 412 (w), ■ 531 (w), ▲ 826 (s), ▲ 870 (sh), ■ 1037 (vs), 1149 (m)	■ C-TiP_2O_7, ▲ $TiV_xP_{2-x}O_7$
c923	243 (m), ■ 277 (vw), ■ 365 (w), ■ 412 (w), ■ 528 (m), ▲ 831 (s), ▲ 875 (sh), ■ 1036 (vs), 1147 (m)	■ C-TiP_2O_7, ▲ $TiV_xP_{2-x}O_7$
c1023	247 (m), ■ 274 (vw), 328 (vw), ■ 367 (w), ■ 415 (w), ■ 532 (m), ▲ 830 (s), ▲ 873 (sh), ■ 1038 (s), 1149 (m)	■ C-TiP_2O_7, ▲ $TiV_xP_{2-x}O_7$

[a] *Note.* vw, very weak; w, weak; m, medium; s, strong; vs, very strong; vb, very broad; sh, shoulder.

the presence of two additional broad bands at ~828 (s) and ~873 (sh) cm^{-1}. Raman bands in vanadium-supported catalysts in the 840- to 600-cm^{-1} region have been assigned to symmetric vibrations of V–O–V groups with dimeric or oligomeric vanadium oxide-type structures. These vanadium species are present in the C-$TiV_xP_{2-x}O_7$ solid solution. Dimeric-type vanadium structures in which vanadium is tetrahedrally coordinated, e.g., ZnV_2O_7 (45) and ZrV_2O_7 (46), have been shown to present Raman bands at similar positions. Crystalline V_2O_5 was not detected in any of the Raman spectra of the catalysts, and higher V loading is required to develop V_2O_5 crystals (15).

Solid-State NMR Spectroscopy

Figure 6 shows the ^{31}P MAS NMR spectra of the α-TiP support, as prepared and calcined at increasing temperatures up to 1123 K. The spectrum of the noncalcined α-TiP (Fig. 6(a)) consists of a peak at −19.5 ppm as well as two very weak signals at ca. −14 and −7 ppm, probably due to the presence of some defects or impurities in the sample. The main peak in the spectrum at ca. −20 ppm is attributed to $(HPO_4)^{2-}$ units in the α-$Ti(HPO_4)_2H_2O$ phase, although it appears slightly shifted to the lower field and shows some asymmetry (47, 48). The α-TiP support calcined at 723 K shows new resonances accompanied by a marked broadening of the spectrum (Fig. 6(b)). This spectrum is mainly formed by a new band centered at −33.5 ppm that, according to the XRD results, must be assigned to $(P_2O_7)^{4-}$ units of ill-crystallized L-TiP_2O_7. In addition, the peak at ca. −20 ppm due to $(HPO_4)^{2-}$ units is broadened, and less intense peaks at −14.0 ppm and −5.5 ppm, as well as a very weak component at ca. 0 ppm due to free H_3PO_4, are evident in Fig. 6(c). In layered titanium phosphates, ^{31}P signals in the range between −5.3 and −10.6 ppm have been previously ascribed to $(H_2PO_4)^-$ and, therefore, the signal at −5.5 ppm must be due to $(H_2PO_4)^-$ groups. Although the resonance at −14.0 ppm appears at a chemical shift intermediate between those of $(H_2PO_4)^-$ and $(HPO_4)^{2-}$ units, we tentatively attribute this to signal to an $(HPO_4)^{2-}$ unit in a different crystallographic site (47, 48). The presence of ^{31}P signals from H_3PO_4 and $(H_2PO_4)^-$ groups indicates that during calcination the water from dehydration hydrolyzes P–O–Ti bonds. This leads to the formation of new Ti–OH and P–OH bonds, which contribute to the lack of crystallization of the L-TiP_2O_7, a situation in agreement with the X-ray diffraction data. The difference in the local

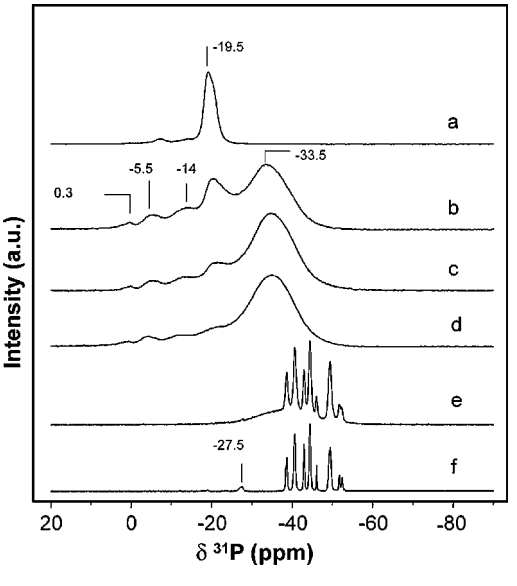

FIG. 6. ^{31}P MAS NMR spectra of samples: (a) α-TiP, (b) α-TiPc723, (c) α-TiPc823, (d) α-TiPc923, (e) α-TiPc1023, and (f) α-TiPc1123.

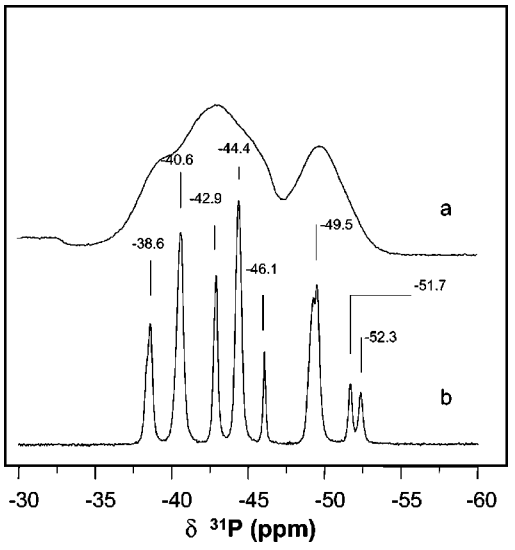

FIG. 7. ^{31}P MAS NMR spectra of samples: (a) c1123 and (b) α-TiPc1123.

environment of $(P_2O_7)^{4-}$ groups in C-TiP_2O_7 with respect to L-TiP_2O_7 must cause the higher field chemical shift. As the calcination temperature is increased up to 923 K, the resonance of the $(P_2O_7)^{4-}$ groups at −33.5 ppm becomes predominant, while the relative intensities of all the peaks appearing at low field progressively decrease, indicating that condensation of H-containing groups is occurring. A dramatic change in the ^{31}P MAS NMR spectrum is observed after calcination of the α-TiP support at 1023 K. The new spectrum consists of sharp peaks in the range −35 to −55 ppm that are superimposed to give a broad band, probably due to $(P_2O_7)^{4-}$ groups of some residual L-TiP_2O_7 or ill-crystallized phase, a situation in agreement with the XRD data. When the α-TiP is calcined at 1173 K, the broad component disappears and a well-resolved spectrum that is characteristic of a crystalline material is obtained. The region of interest is expanded in Fig. 7(b) and shows nine resonances that coincide with those of cubic TiP_2O_7 (48, 49), which is based on the arrangement of octahedral TiO_6 sharing corners with P_2O_7 groups. The 9 ^{31}P peaks correspond to 11 phosphorus crystallographic sites, as concluded from two-dimensional (2D) MAS NMR experiments (50). The presence of a very weak band at −27.5 ppm in the spectrum in Fig. 6(f) will be discussed in the following.

The ^{31}P MAS NMR spectra of the vanadium-containing catalysts submitted to calcination temperatures in the range 723–1123 K are shown in Fig. 8. The spectrum of the catalyst calcined at 723 K is very broad and featureless. As shown in Fig. 8(a), the contribution of two bands centered at −33 ppm, due to $(P_2O_7)^{4-}$ groups, and at −25 ppm, which is tentatively assigned to $(HPO_4)^{2-}$ groups, is consistent with the formation of a layered titanium pyrophosphate phase. Raman and ^{51}V NMR data (vide infra) suggest the presence of a $VOPO_4$ phase that could be obscured by the other signals in the ^{31}P MAS NMR spectrum (44). The absence of the lower field peaks, which were observed for the α-TiPc723 sample, indicates that the layered phase formed in the presence of vanadium is not exactly the same. Inspection of the spectrum of sample c723 shows a high-field asymmetry at ca. −43 ppm, which may indicate the presence of cubic titanium pyrophosphate with low crystallinity (as seen by XRD). When the catalyst is calcined at 823 K, the spectrum is dominated by a broad resonance centered at −43.5 ppm with two shoulders at ca. −40 and −49 ppm, as well as some contribution at −33 ppm (Fig. 8(b)). As the calcination temperature is raised, this latter component, which can be ascribed to residual layered titanium pyrophosphate, decreases while the main signals at high field become slightly better defined (see Fig. 8).

To compare the ^{31}P MAS NMR spectra of the catalysts calcined at 823 K or higher, Fig. 7 shows the spectra of sample c1173 and that of α-TiPc1173, which is typical of a cubic titanium pyrophosphate. Although the V-containing catalyst c1173 does not give sharp resonances in this spectral region, its shape reproduces the envelope of the peaks in Fig. 7(b), suggesting the formation of a cubic TiP_2O_7-like structure, a situation in agreement with the XRD results. The lack of resolution in the spectra of the calcined catalysts is consistent with a range of ^{31}P chemical shifts, indicating the occurrence of phosphorus in slightly different environments. On the basis of the XRD data shown in Fig. 3a, this phenomenon could be due to local distortions caused by the incorporation of V atoms in structural sites.

Moreover, a weak and narrow peak at ca. −27.5 ppm appears when the catalyst is calcined at 823 K (sample c823). This peak increases with increasing calcination temperature and becomes particularly intense in catalyst c1173. The

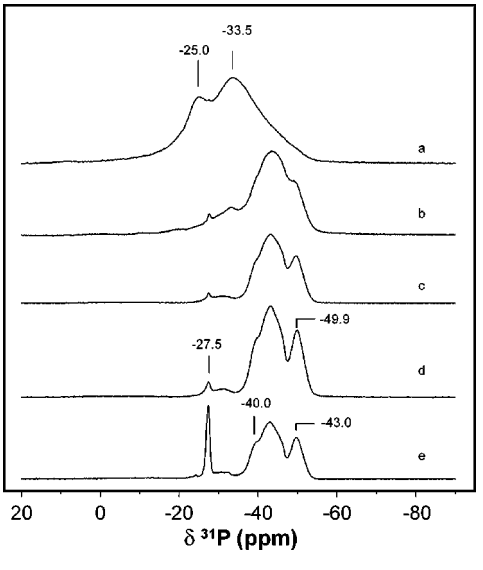

FIG. 8. ^{31}P MAS NMR spectra of samples: (a) c723, (b) c823, (c) c923, (d) c1023, and (e) c1123 K.

assignment of this peak to a specific phosphate phase is not definite, but it cannot be assigned to a V–P–O phase because it also appeared in the bare support (see Fig. 6(e and f)). The peak may be related to a new titanium phosphate phase with a higher P/Ti stoichiometry developed from C-TiP_2O_7 at high-temperature calcination. The phase change in the Ti–P–O system promoted by V, as well as the migration of P to surface induced by P–V exchange, may explain the higher concentration of this phase in the catalysts c823, c923, 1023, and c1123.

Figure 9 shows the ^{51}V wide-line and MAS NMR spectra of the catalyst calcined in the temperature 723–1123 K range. Although the ^{51}V nucleus ($I = 7/2$) is quadrupolar, it has been shown that the shape of the nonspinning spectra is usually dominated by the chemical shift anisotropy, which allows information to be obtained regarding the symmetry environment of the vanadium center. Very often, the nature of the vanadium species is determined from the wide-line rather than from the spinning spectra. The static ^{51}V spectrum of sample c723, which is shown in Fig. 9(a), consists mainly of a signal exhibiting axial symmetry with $\delta_{11} = \delta_{22} = \delta_{\perp} = -300$ ppm and $\delta_{33} = \delta_{//} \approx -900$ ppm, a $\Delta\delta = |\delta_{11} - \delta_{33}| \approx 600$ ppm, and a δ_{iso} (indicated in the figure) estimated as $(\delta_{11}+\delta_{22}+\delta_{33})/3$. Nevertheless, we cannot rule out some contribution of the band centered at −750 ppm, which dominates the spectrum of catalyst c823 (Fig. 9(b)). The value of $\Delta\delta$ increases with the anisotropy of the chemical shift and is a measure of the distortion of the vanadium site. The parameters of the dominant signal in Fig. 9(a) are typical of V^{5+} in an axially symmetric octahedral coordination (51) but are different from those reported for V_2O_5 (51). This fact allows us to rule out the presence of a supported oxidic phase in sample c723. The spectra in Fig. 9 (a) (a′) can be attributed to $VOPO_4$. However, the assignment of these spectra to a specific phase is not straightforward. A signal with $\delta_{\perp} = -285$ ppm and $\delta_{//} \approx -1547$ ppm has been previously reported for $VOPO_4$ (51), but the structural type was not specified. ^{51}V wide-line spectra of α_{II}-$VOPO_4$ have been reported to give complex patterns with three maxima at −77, −316, and −592 ppm, while β-, γ-, and δ-$VOPO_4$ give essentially one peak at about −354, −300, and −284 ppm, respectively (44). The spectra reported for the $VOPO_4$ phases differ from that in Fig. 9(a), although the shape of the static spectra can be affected by the acquisition parameters. On comparing the wide-line and spinning spectra of sample c723 to those for α_{II}-, β-, γ-, and δ-$VOPO_4$, it can be seen that the spectrum of c723 show more similarities to those of γ-$VOPO_4$. However, a definite conclusion about the specific $VOPO_4$ phase detected by NMR cannot be reached. Since Raman spectroscopy detected α_{II}-$VOPO_4$, we can tentatively assign the main ^{51}V signal in the spectra in Fig. 9 (a, a′) to this phase. The spectrum of the catalyst calcined at 823 K shows a contribution of the component at −300 ppm and a new band, centered at −750 ppm, that also displays shoulders. The spinning spectrum is formed by the superposition of a spinning sideband pattern and of broad bands. This suggests the contribution of an ill-crystallized phase.

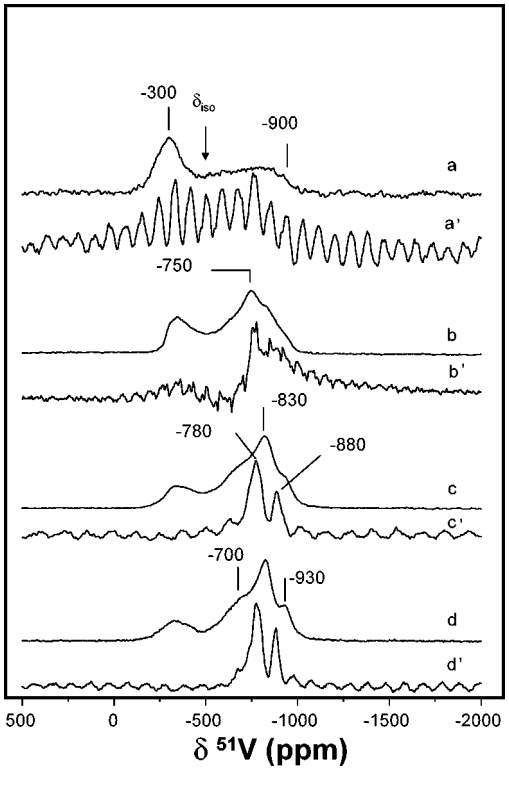

FIG. 9. ^{51}V wide-line (a–d) and MAS (a′–d′) NMR spectra of samples: (a, a′), c723; (b, b′), c823; (c, c′), c923; and (d, d′), c1023.

As the calcination temperature is increased to 923 K, the maximum in the high-field part of the spectrum appears at ca. −830 ppm. When the sample is spun, the signals become narrower and a set of low-intensity spinning sidebands appears in the spectrum. The low-field signal at ca. −300 ppm can tentatively be attributed to some residual $VOPO_4$ or, in any case, to V^{5+} in an octahedral coordination environment. Although the anisotropic shape of the signals contributing to the band centered at −830 ppm are not distinguishable, the position of the shoulders strongly suggests that the chemical anisotropy $\Delta\delta$ must be lower than 300 ppm. This is usually the case for dimeric V^{5+} species in a slightly distorted tetrahedral coordination (51). The appearance of two new peaks during spinning indicates the presence of two nonequivalent tetrahedral V^{5+} species. Assuming this assignment to be correct, the ^{51}V spectra of the catalysts calcined at temperatures above 823 K would support the incorporation of vanadium within the cubic TiP_2O_7 structure.

XPS

To determine the relative vanadium concentration on the catalyst surface and, therefore, if V spreads over the surface of the Ti phosphate support, the surface chemical

composition was measured by XPS. Table 3 provides the V/Ti and P/Ti ratios of the catalysts, as determined by XPS, as well as the bulk ratios obtained from chemical analysis. The surface P/Ti ratio of the catalyst determined by XPS is, in all cases, higher than that obtained from bulk composition and increases with the calcination temperature. This indicates that the catalyst surface is enriched in P and that this enrichment is more marked at higher calcination temperatures.

The V/Ti surface ratio in c723 is only slightly higher than that of the bulk, indicating that the V-containing $VOPO_4$ crystals do not cover the Ti phosphate support, but rather form a physical mixture of the two phases (15). As the calcination temperature of the catalyst is raised, the V/Ti surface ratio increases and, after the treatment at 1023 K, becomes four times larger than that at 723 K. The XPS V/Ti augmentation can be explained in terms of the formation of the cubic solid solution in which V is atomically dispersed throughout the bulk. The increase in the XPS V/Ti ratio cannot be explained by the spreading of a V (or VPO) phase on the surface of the Ti phosphate; otherwise a dispersed V phase would have been detected by any of the other characterization techniques employed. The XPS V/Ti values of c823, c923, and c1023 suggest that the surface is covered by a cubic $TiV_xP_{2-x}O_7$ solid solution in which the V is "atomically" dispersed and the V stoichiometry progressively increases upon the calcination temperature. The solid solution is not the only phase present at the surface: a Ti–P–O phase with a high P/Ti ratio must coexist, as suggested by the ^{31}P MAS NMR results (peak at −27.5 ppm for the catalysts and support calcined at high temperatures) and XPS data (see following).

Catalytic Tests

Figures 10 and 11 show the results for the oxidation of *o*-xylene on different catalysts. Bare supports are much less active and selective than their V-containing counterparts (not shown in the figures). *o*-Xylene is transformed to partially oxidized products and, if the oxidation proceeds to a greater extent, to carbon oxides. Among the partially oxidized products, *o*-tolualdehyde (*o*-TAL), phthalic anhydride (PA), and phthalide (PL) are the major products. The selectivity to PA (the product of interest) increases smoothly with temperature to the detriment of the selectivities in *o*-TAL and PL: *o*-TAL and PL are oxidized to PA as conversion rises, a situation that has also been reported in the literature (13). The loss of carbon balance was significant (between 15 and 25%) at higher conversion on previous V/α-TiP catalysts (15). A deposit of heavy products was observed at the bottom of the reactor (the cooler zone of the glass reactor), upstream from the condensation trap. This zone is heated at temperatures higher than 600 K, and hence the observed products must be nonvolatile and are very likely to result from the condensation of aromatic

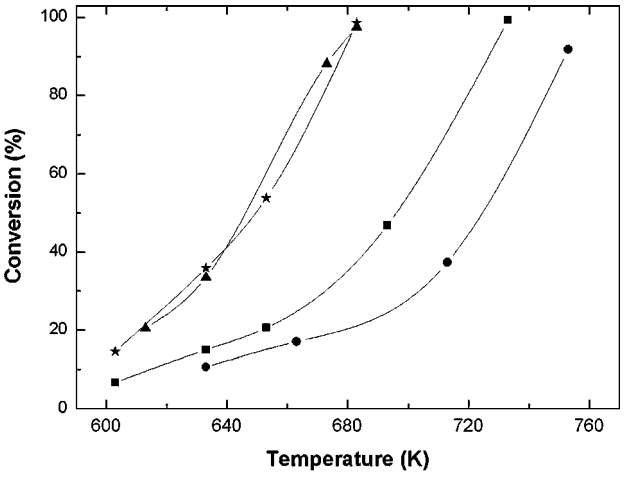

FIG. 10. *o*-Xylene conversion for catalysts: ▲, c723; ★, c823; ■, c923; and ●, c1023.

rings (heavy polyaromatic rings) (52–55). Upon increasing the W/F ratio, the formation of such products was considerably reduced and, consequently, the carbon balance (defined as the ratio between inlet C and outlet carbon × 100) significantly improved (loss of carbon balance between 5 and 10%) with respect to previous experiments. Conversion increases with temperature in all catalysts (see Fig. 10). Catalysts c723 and c823 K are the most active: the temperature needed to achieve total conversion is much lower than for the catalysts calcined at higher temperatures, i.e., c923 and c1023.

The PA selectivity–conversion profiles (Fig. 11) provide information about the selectivity of the surface. The c723 catalyst is the most selective sample and, upon increasing the temperature of calcination, the PA selectivity at isoconversion compares unfavorably to that associated with the c723 catalyst. It is clear that the higher the calcination temperature, the lower the PA selectivity. This decrease in the

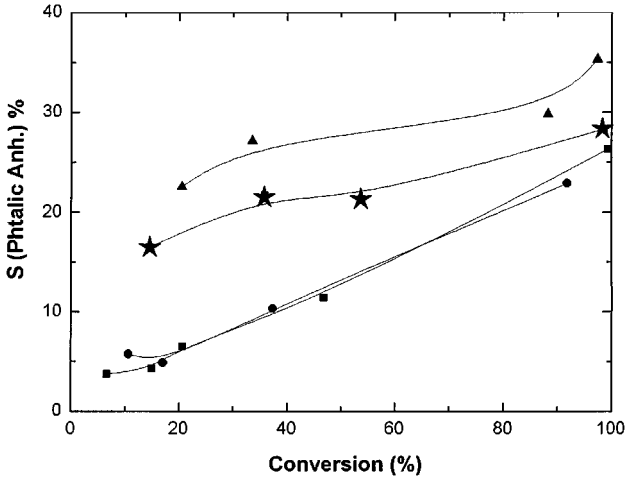

FIG. 11. Selectivity to phthalic anhydride vs conversion profiles: ▲, c723; ★, c823; ■, c923; and ●, c1023.

PA selectivity is clearly evident in Fig. 11, which compares PA selectivity at isoconversion. Catalysts calcined at higher temperatures are less active, and therefore the PA productivity, for a given temperature, is much lower for c923 and c1023 catalysts. It is clear that the rise in calcination temperature brings about remarkable changes in the catalytic properties of the V/α-TiP catalysts.

DISCUSSION

The formation of a solid solution by substitution of tetrahedral phosphorus by vanadium cations in cubic pyrophosphate was clearly revealed by XRD. ^{51}V NMR data and Raman spectroscopy provide further support for this phenomenon. Similar Raman features to those at ~828 (s) and ~873 (sh) cm^{-1} were assigned to V–O–V symmetric stretching vibrations detected in phases like ZnV_2O_7 (45) and ZrV_2O_7 (46). In these compounds, vanadium is tetrahedrally coordinated to form a dimeric V_2O_7-type, and this structure indicates that V substitutes are, to a great extent, both phosphorous of $(P_2O_7)^{4-}$ units.

The formation of the solid solution occurs progressively as the temperature of calcination is increased, as evidenced by the continuous variation of many of the chemical and physical parameters determined by the characterization techniques used in this study. However, it is surprising that the unit cell expansion evidenced by XRD analysis is more intense in the catalyst calcined at the lower temperature. Such an effect can be explained as follows. At very low calcination temperatures, the V phase is not well dispersed over the support surface, and the overall solid can be understood as a mixture of Ti phosphate and very small crystals of V phase. Only the part of the phosphate support in close contact with the V phase will undergo the transformation to cubic pyrophosphate with the subsequent isomorphic substitution. Although the amount of cubic solid solution is locally low, the V concentration (x value) in the solid solution will be high, thus leading to the relatively high expansion of the C-$TiV_xP_{2-x}O_7$ unit cell detected by XRD. At higher calcination temperatures, the formation of the solid solution progresses in the phosphate crystal by thermal activation. Therefore, the domain of the solid solution grows while the local x value becomes slightly smaller, and consequently, the expansion of the unit cell is less severe though still clearly visible. Indeed, it seems that the solid solution affects all of the solid when calcination occurs at 1173 K.

Although there is a remarkable migration of P to the surface when V catalysts are calcined at increasingly higher temperatures (c823, c923, c1023, and c1123), P_2O_5 is not detected by any of the characterization techniques used. ^{31}P MAS NMR could even detect very amorphous P_2O_5, arising from H_3PO_4, as a peak at ca. 0 ppm. P_2O_5 is a very hygroscopic material and results in the formation of H_3PO_4 when it reacts with water. (NMR spectra were recorded in an atmosphere of air.) The formation of an amorphous Ti phosphate that is much richer in P than in $Ti_2P_2O_7$ could occur and not be detected by any of the techniques used in this work. Additional ^{31}P NMR peaks can be obscured by the broad bands present in the spectra between −35 and −55 ppm in c823, c923, c1023, and c1123 samples. Moreover, the ^{31}P MAS NMR peak at −27.5 ppm can be assigned to this P environment, though additional work would be required to confirm this unequivocally.

The increase in the calcination temperature results in a clear decrease in the specific area of the catalysts. The decrease in the specific area could be a consequence of the better crystallization of the cubic solid solution. V promotes the formation of the cubic phase at lower temperatures, a situation that results in comparably better crystallization than in the V-bare C-TiP_2O_7 phase. The decrease in the specific area accounts for the remarkable decrease in catalytic activity for c923 and c1023, although the relative surface enrichment in V concentration, as detected by XPS, could have been expected to result in more active catalysts. As far as the PA selectivity is concerned, this significantly deteriorates (at isoconversion) when catalysts are calcined at higher temperatures. The characterization techniques employed reveal that the phases and, in particular, the chemical composition of the surface of the catalysts markedly change during calcination. A physical mixture of the α_{II}-$VOPO_4$ and L-TiP_2O_7 phases predominates in c723. (A small fraction of C-$TiV_xP_{2-x}O_7$ is visible by XRD and Raman spectroscopy.) When the calcination temperature is increased, two features characterize the surface: the relative P and V enrichment and the presence of a C-$TiV_xP_{2-x}O_7$ solid solution along with a P-rich Ti phosphate. To assign the decline of the PA selectivity to any of these factors is not straightforward because both can cause such a tendency. The increase in Brønsted acidity associated with the P enrichment could cause a serious decrease of the PA selectivity. On the other hand, the tetrahedrally coordinated V species present in the cubic solid solution does not show the same coordination as the most selective vanadium species existing in the best catalysts so far, i.e., V_2O_5/TiO_2, which consists of layers of amorphous vanadium oxide in which vanadium shows an octahedral coordination.

The formation of the cubic $TiV_xP_{2-x}O_7$ solid solution at a much lower temperature than C-TiP_2O_7 indicates that the solid solution is more stable. It can be assumed that the substitution of P^{5+} by V^{5+} imparts stability to the cubic phase and that the phase change is a favored process. If one accepts this assumption, interesting speculations can be considered regarding such systems. It can be envisaged, for example, that similar phenomena could take place in the Ti-phosphate domains of industrial catalysts. This possibility is supported by the fact that industrial catalysts, based on $V_2O_5/TiO_2(a)$, contain P as an impurity that is largely concentrated at the TiO_2 surface (13), and that Ti phosphate is developed by the addition of P to TiO_2 (32).

An initial question prompted by the data presented here concerns the effect that calcination temperature may induce on $V_2O_5/TiO_2(a)$ catalysts. The data presented in this work indicate that an increase in the calcination temperature of $V_2O_5/TiO_2(a)$ may induce a segregation of bulk P to the surface by exchange with surface V, thus enhancing the concentration of nondesirable Brønsted P–OH sites at the surface. The consequence of calcination of $V_2O_5/TiO_2(a)$ at higher temperatures may be the deterioration of the PA selectivity.

The second question that raises concerns about whether the V^{5+} that has been detected by both XPS (56) and electrical conductivity measurements (57) to be dissolved into the $TiO_2(a)$ lattice can be driven by the exchange of the P^{5+} bulk impurities by V^{5+} cations. However, the conductivity in the $V_2O_5/TiO_2(a)$ system is explained by the presence of an excess of delocalized electrons associated with the insertion of pentavalent V^{5+} cations in a tetravalent Ti^{4+} environment. In this case the delocalized electrons can be easily ionized into the conduction band with a very small thermal activation energy (57). Tetrahedral P^{5+} substitution by tetrahedral V^{5+}, as described in the system presented in this work, cannot, in principle, create conductive electrons. This fact contradicts the theory presented earlier, unless it is assumed that the V^{5+} cations dissolved in the bulk anatase, as detected by conductivity measurements (57), are (i) not driven by a V–P exchange mechanism but by a different one and (ii) only represent a fraction of V^{5+} cations detected by XPS (56).

CONCLUSIONS

The findings of this study indicate that vanadia cannot be supported as two-dimensional overlayers on L-TiP_2O_7 and C-TiP_2O_7. The addition of V promotes the laminar-to-cubic phase transition, which results in the formation of a C-$TiV_xP_{2-x}O_7$ solid solution with P segregation to the surface of the solid. The solid solution brings about the deactivation of the catalyst by the decrease of the specific area. In addition, the catalysts obtained by calcination at high temperature are less selective to the oxidation of *o*-xylene to PA.

ACKNOWLEDGMENTS

Financial support from CICYT, Spain, under Project MAT96-2058-CE and from the Commission of the European Union BRPR-CT95-0062 is gratefully acknowledged. We thank Dr. J. M. Amarilla for assistance and helpful discussions on XRD data.

REFERENCES

1. Miki, J., Osada, Y., Konoshi, T., Tachibana, Y., and Shikada, T., *Appl. Catal. A Gen.* **137**, 93 (1996).
2. Van Hengstum, A. J., Pranger, J., Van Ommen, J. G., and Gellings, P. J., *Appl. Catal.* **11**, 317 (1984).
3. Zhu, J., Rebenstorf, B., and Andersson, S. L. T., *J. Chem. Soc., Faraday Trans. I* **85**, 3645 (1989).
4. Nikolov, V., Klissurski, D., and Anastasov, A., *Catal. Rev.—Sci. Eng.* **33**, 319 (1991).
5. Santamaría-González, J., Martínez-Lara, M., Bañares, M. A., Martínez-Huerta, M. V., Rodríguez-Castellón, E., Fierro, J. L. G., and Jiménez-López, A., *J. Catal.* **181**, 280 (1999).
6. Roy, M., Gubelmann-Bonneau, M., Ponceblanc, H., and Volta, J. C., *Catal. Lett.* **42**, 93 (1996).
7. Tessier, L., Bordes, E., and Gubelmann-Bonneau, M., *Catal. Today* **24**, 335 (1995).
8. Overbeek, R. A., Warringa, P. A., Crombag, M. J. D., Visser, L. M., van Dillen, A. J., and Geus, J. W., *Appl. Catal. A Gen.* **135**, 209 (1996).
9. Wachs, I. E., Jehng, J.-M., Deo, G., Weckhuysen, B. M., Guliants, V. V., Benziger, J. B., and Sundaresan, S., *J. Catal.* **170**, 75 (1997).
10. Busca, G., Marchetti, L., Centi, G., and Trifirò, F., *Langmuir* **2**, 568 (1986).
11. Centi, G., *Appl. Catal.* **147**, 267 (1996).
12. Dias, C. R., and Farinha Portela, M., *Catal. Rev. Sci. Eng.* **39**, 169 (1997).
13. Andersson, S. L. T., *J. Chem. Soc., Faraday Trans. I* 1537 (1986).
14. Sato, T., Nakanishi, Y., Maruyama, K., and Suzuki, T., U.S. Patent 4,481,304 (1984).
15. Del Val, S., López Granados, M., Fierro, J. L. G., Santamaría-González, J., Jiménez-López, A., *J. Catal.* **188**, 203 (1999).
16. Deo, G., and Wachs, I. E., *J. Catal.* **146**, 335 (1994).
17. Zhu, J., Rebenstorf, B., and Andersson, S. L. T., *J. Chem. Soc., Faraday Trans. 1* **85**, 3645 (1989).
18. Centi, G., López Granados, M., Pinelli, D., and Trifirò, F., *Stud. Surf. Sci. Catal.* **67**, 1 (1991).
19. Grzybowska-Swierkosz, B., *Appl. Catal.* **157**, 263 (1997).
20. Centi, G., López Granados, M., Pinelli, D., and Trifirò, F., *Stud. Surf. Sci. Catal.* **67**, 1 (1991).
21. Centi, G., Giamello, E., Pinelli, D., and Trifirò, F., *J. Catal.* **130**, 220 (1991).
22. Centi, G., Pinelli, D., Trifirò, F., Ghoussoub, D., Guelton, M., and Gengembre, L., *J. Catal.* **130**, 238 (1991).
23. Deo, G., Wachs, I. E., and Haber, J., *Criti. Rev. Surf. Chem.* **4**, 141 (1994).
24. Inumaru, K., Misono, M., and Okuhara, T., *Appl. Catal. A Gen.* **149**, 133 (1997).
25. Bond, G. C., and Tahir, S. F., *Appl. Catal.* **71**, 1 (1991).
26. Bond, G. C., Zurita, J. P., Flamerz, S., Gellings, P. J., Bosch, H., van Ommen, J. G., and Kip, B. J., *Appl. Catal.* **22**, 361 (1986).
27. Xue, Z.-Y., and Schrader, G. L., *J. Phys. Chem. B* **103**, 9459 (1999).
28. Bortun, A. I., Khainakov, S. A., Bortun, L. N., Poojary, D. M., Rodriguez, J., Garcia, J. R., and Clearfield, A., *Chem. Mater.* **9**, 1805 (1997).
29. Bordes, E., *Catal. Today* **1**, 499 (1987).
30. Bereznitski, Y., Jaroniec, M., Bortun, A. I., Poojary, D. M., and Clearfield, A., *J. Colloid Interface Sci.* **191**, 442 (1997).
31. Krogh Andersen, A. M., and Norby, P., *Inorg. Chem.* **37**, 4313 (1998).
32. Soria, J., Conesa, J. C., López Granados, M., Mariscal, R., Fierro, J. L. G., García de la Banda, J. F., and Heinemann, H., *J. Catal.* **120**, 457 (1989).
33. Clearfield, A., and Thakur, D. S., *Appl. Catal.* **26**, 1 (1986).
34. Tegehall, P. E., *Acta Chem. Scand.* **40**, 507 (1986).
35. Bruque, S., Aranda, M. A. G., Losilla, E., Olivera-Pastor, P., and Maireles-Torres, P., *Inorg. Chem.* **34**, 893 (1995).
36. Slade, R. C. T., Knowles, J. A., Jones, D. J., and Rozière, J., *Solid State Ionics* **96**, 9 (1997).
37. Ramis, G., Busca, G., Lorenzelli, V., La Ginestra, A., Galli, P., and Masucci, M. A., *J. Chem. Soc., Dalton Trans.* 881 (1998).
38. Wagner, C. D., Davis, L. E., Zeller, M. V., Taylor, J. A., Raymond, R. H., and Gale, L. H., *Surf. Interface Anal.* **3**, 211 (1981).

39. Sing, K. S. W., Everett, D. H., Haul, R. A. W., Moscou, L., Pierotti, R. A., Rouquerol, J., and Siemieniewska, T., *Pure Appl. Chem.* **57**, 603 (1985).
40. Nørlund Christensen, A., Krogh Andersen, E., Krogh Andersen, I. G., Alberti, G., Nielsen, M., and Lehmann, M. S., *Acta Chem. Scand.* **44**, 865 (1990).
41. McMurdie, H. F., Morris, M. C., Evans, E. H., Paretzkin, B., Wong-Ng, W., Zhang, Y., and Hubbard, C. R., *Powder Diff.* **2**, 52 (1987).
42. Korthuis, V., Khosrovani, N., Sleight, W., Roberts, N., Dupree, R., and Warren, Jr., W. W., *Chem. Mater.* **7**, 412 (1995).
43. Deo, G., Wachs, I. E., and Haber, J., *Critic. Rev. Surf. Chem.* **4**, 141 (1994).
44. Ben Abedlouahab, F., Olier, R., Guilhaume, N., Lefebvre, F., and Volta, J. C., *J. Catal.* **134**, 151 (1992).
45. Vuurman, M. A., and Wachs, I. E., *J. Phys. Chem.* **96**, 5008 (1992).
46. Sanati, M., Andersson, A., Wallenberg, L. R., and Rebenstorf, B., *Appl. Catal. A Gen.* **106**, 51 (1993).
47. Li, Y. J., and Wittingham, M. S., *Solid State Ionics* **63–65**, 391 (1993).
48. Bortun, A. I., Bortun, L., Clearfield A., Villa-García, M. A., García, J. R., and Rodríguez, J., *J. Mater. Res.* **11**, 2490 (1996).
49. Sanz, J., Iglesias, J. E., Soria, J., Losilla, E. R., Aranda, M. A. G., and Bruque, S., *Chem. Mater.* **9**, 996 (1997).
50. Helluy, X., Marichal, C., Sebald, A., *J. Phys. Chem. B* **104**, 2836 (2000).
51. Lapina, O. B., Mastikhin, V. M., Shubin, A. A., Krasilnikov, V. N., and Zamarev, K. I., *Prog. Nucl. Magn. Reson. Spectrosc.* **24**, 457 (1992).
52. Andersson, S. L. T., *J. Catal.* **9**, 138 (1986).
53. Dias, C. R., Farinha Portela, M., and Bond, G. C., *J. Catal.* **157**, 344 (1995).
54. Dias, C. R., Farinha Portela, M., and Bond, G. C., *J. Catal.* **157**, 353 (1995).
55. Dias, C. R., Farinha Portela, M., and Bond, G. C., *J. Catal.* **162**, 284 (1995).
56. Nogier, J. Ph., De Kersabiec, A. M., and Fraissard, J., *Appl. Catal. A Gen.* **185**, 109 (1999).
57. Vedrine, J., Ed., *Catal. Today* **20**, 135 (1994).